



On an acoustics–thermal–fluid coupling model for the prediction of temperature elevation in liver tumor

Tony W.H. Sheu ^{a,b,*}, Maxim A. Solovchuk ^a, Alex W.J. Chen ^a, Marc Thiriet ^c

^a Department of Engineering Science and Ocean Engineering, National Taiwan University, No. 1, Sec. 4, Roosevelt Road, Taipei 10617, Taiwan, ROC

^b Taida Institute of Mathematical Science (TIMS), National Taiwan University, Taiwan, ROC

^c LJLL, University of Paris # 6, Paris, France

ARTICLE INFO

Article history:

Received 17 September 2010

Received in revised form 24 February 2011

Accepted 24 February 2011

Available online 5 May 2011

Keywords:

Liver tumor

Acoustics–thermal–fluid

HIFU

Perfusion

Blood convective cooling

Acoustic streaming

ABSTRACT

The present study is aimed at predicting liver tumor temperature during a high-intensity focused ultrasound (HIFU) thermal ablation using the proposed acoustics–thermal–fluid coupling model. The linear Westervelt equation is adopted for modeling the incident finite-amplitude wave propagation. The non-linear hemodynamic equations are also taken into account in the simulation domain that contains a hepatic tissue domain, where homogenization dominates perfusion, and a vascular domain, where blood convective cooling may be essential in determining the success of HIFU. Energy equation for thermal conduction involves two heat sinks to account for tissue perfusion and forced convection-induced cooling. The effect of acoustic streaming is also included in the development of the current HIFU simulation study. Convective cooling in large blood vessel and acoustic streaming were shown to change the temperature near blood vessel. It was shown that acoustic streaming effect can affect the blood flow distribution in hepatic arterial branches and leads to the mass flux redistribution.

© 2011 Elsevier Ltd. All rights reserved.

1. Introduction

Our liver is a highly perfused organ with the blood supply from the hepatic artery and the portal vein [1]. This organ has the functions to secret bile, store glycogen, distribute nutrients from the blood and gastrointestinal tract. In addition, it can also get rid of endogenous/exogenous substrates and toxins. Such a physiologically complex and important organ is unfortunately susceptible to primary and metastatic malignant diseases. In Taiwan, each year more than 7000 adults died of the primary hepatocellular carcinoma (HCC) mainly (or 80%) due to liver cirrhosis [2] and metastatic colorectal liver carcinoma. Statistically, liver cancer is now ranked as the second leading cause of death [3]. More than one million deaths were also reported to be in association with the primary and metastatic malignancies worldwide [4].

Surgical resection of primary and metastatic hepatic tumors remains nowadays as the golden standard of therapy [5]. Quite a few patients with cirrhosis are, unfortunately, not suitable for surgical resection due to their multifocal disease, tumor size, and tumor location [6]. As a result, other alternative means such as the hepa-

tic artery infusion chemotherapy, percutaneous ethanol injection (PEI), cryotherapy, microwave coagulation therapy (MCT) and laser induced thermotherapy (LITT) [7] have been developed. Due to some inevitable adverse side effects, none of these therapies have yet been demonstrated to be the long-term survival treatment. Rapid ablation of the tumor tissues, aided either by percutaneous image-guided CT, MRI or ultrasound, is also possible by the thermal energy generated from the high-frequency radio-frequency (RF) [8,9]. Although RF thermoablative therapy is now one of the promising minimally invasive means to replace open laparotomy, the problem regarding the accompanied higher recurrence rate than the hepatic resection has not been fully resolved. Development of some planning tools so as to enable an accurate and efficient ablation of tumors without over-heating the healthy tissues in close proximity to the RF probe is still in strong demand [10].

Energy generated by ultrasound has been applied for several decades to safely image the body interior without the risk of damaging tissues at a comparatively low power of ionizing radiation. Use of ultrasound energy with a proper amount has also been proposed to destroy concretions in biliary (cholelithiasis) and in urinary (urolithiasis) tract. With the rapid technological advancement of an increasingly wider piezoelectric array, a higher power ultrasound has also been recently put to clinical use in therapeutic and surgical applications by depositing heat over some highly targeted areas in human body. Ultrasound in clinic practice has been reported to have some potentially beneficial bioeffects in sealing

* Corresponding author at: Department of Engineering Science and Ocean Engineering, National Taiwan University, No. 1, Sec. 4, Roosevelt Road, Taipei 10617, Taiwan, ROC. Tel.: +886 2 33665746; fax: +886 2 23929885.

E-mail addresses: twhsheu@ntu.edu.tw (T.W.H. Sheu), solovchuk@gmail.com (M.A. Solovchuk).

Nomenclature

c_0	speed of ultrasound in tissue (m/s)	y	coordinate in the y direction
c	specific heat (J/kg °C)	z	coordinate in the z direction
\mathbf{F}	force vector per unit volume (N/m ³)	<i>Greek symbols</i>	
k	the wave number	α	absorption coefficient (Np/MHz m)
k_t	thermal conductivity of tissue (W/m °C)	β	nonlinearity coefficient
I	sound intensity (W/m ²)	δ	acoustic diffusivity
p	acoustic pressure (N/m ²)	λ	wavelength (m)
\mathbf{P}	static pressure (N/m ²)	μ	shear viscosity of blood flow (kg/m s)
q	ultrasound power deposition (W/m ³)	ρ	density (kg/m ³)
t	time (s)	Ψ	acoustic velocity potential
t_0	initial time (s)	ω	angular frequency (MHz)
t_{final}	final time (s)	<i>Subscripts</i>	
T	temperature (°C)	t	tissue
u	velocity (m/s)	b	blood
w_b	blood perfusion rate (kg/m ³ s)		
x	coordinate in the x direction		

blood vessels, dissolving blood clots (thrombolysis), activating drug delivery, opening blood-brain barrier, and increasing cell membrane and skin permeability to molecules [11]. We will consider in this paper only the high-intensity ultrasound, which has been applied with great success to destroy tumor cells.

Ultrasound enables atoms to move in unison to generate a mechanical wave, which can in turn be delivered to the targeted region that is as small as a rice grain. In tissues where ultrasound wave propagates through, one can observe the attenuated and absorbed ultrasound waves. The amount of the energy loss by absorption will be mostly transformed into the thermal energy and this can quickly elevate the medium temperature. With the ultrasound beam being focused, thermal energy can be added primarily to a small region of tissues with little or no deposition at all on the surrounding tissues due to the incident high-intensity focused ultrasound. Through the absorption mechanism, tissue temperature will be elevated to a relatively high magnitude and this local high temperature can cause the thermal coagulation and ablation of cells to occur. The ability of the ultrasound that can safely penetrate deep into the tissues and locally elevate the temperature in a small focal area under proper selection makes it appealing for use in the non-invasive surgical treatment.

HIFU therapy has been used to ablate a variety of solid tumors in different areas of the body [12]. Clinical trials have been recently conducted to evaluate the safety and effectiveness of high-intensity focused ultrasound for the treatment of hepatocarcinoma (HCC) [13,14]. For the safety and efficacy reasons, Wu et al. [13,14] recommended using a 0.8 MHz spherical single-element focused ultrasound transducer (HAIFU Technology Company, Chongqing, China) for patients with HCC. The safety and feasibility of extracorporeal high-intensity focused ultrasound for the treatment of liver tumors has also been independently confirmed by Kennedy et al. [15,16] and Wang [17]. HIFU can also enhance a systemic antitumor cellular immunity in addition to the local tumor destruction in patients with solid malignancies [18], that may increase the cure of carcinoma.

Treatment becomes complicated when the liver tumor is very close to large blood vessels. Quite recently [19] it was first shown that HIFU can safely archive a virtually complete necrosis of tumors close to major blood vessels. Thirty nine patients were treated with the averaged tumor size 7.36 cm. The distance between the tumor and major blood vessels was less than 1 cm. Vascular walls were not damaged during the treatment. These patients deemed not to be surgically respectable, nor suitable for RFA

(Radiofrequency ablation) or PEI (percutaneous ethanol injection) due to the location of the tumor. After a single session of HIFU treatment, the rate of complete necrosis was about 50%. While substantial, this rate of necrosis following HIFU ablation is not completely satisfactory. Lack of a complete response can be explained by the large tumor size and the cooling effects from large vessels. A basic understanding of the factors that can influence necrosis lesion size is necessary for the future improvement of the thermoablative treatment technique. Since numerical prediction approach has enjoyed quite a success for years in many fields of science and engineering, simulation can also play a potentially crucial role in inducing a rapid and invisible thermal necrosis of the malignant tumors whilst minimizing damage in the intervening path.

With the spatially-dependent ultrasonic deposited power, thermal dose will be increased on the medium surface. This will, in turn, elevate the medium temperature. In the past, temperature elevation in soft tissues was mostly modeled by the diffusion-type equation, known as the Pennes bioheat transfer equation, which involves heat source produced by the incident acoustic wave and heat sink owing to perfusion in capillaries [20]. The amount of removed heat can be estimated by averaging the effect of blood perfusion over all the tissues. Homogenization assumption is probably no longer valid in modeling the temperature elevation in regions containing some sufficiently large vessels, inside which the blood is flowing. Both biologically relevant convective cooling in large blood vessels and perfusion cooling in microvasculatures need to be taken into account altogether. Inclusion of these two possible cooling means will greatly increase the modeling complexity since the equations of motion for blood flow need to be solved together with the divergence-free velocity constraint equation. Curra et al. [21] developed a model to determine the influence of blood flow on the dimensions of the temperature distribution in the tissue during the focused ultrasound surgery. Their model was based on the nonlinear acoustic equation and the bioheat equation. The blood vessel was on the acoustic axis. Hariharan et al. [22] studied the influence of large blood vessels on the lesion size. In the computations he firstly considered the case with ultrasound beam propagating in a direction parallel to the blood vessel. In the second, ultrasound beam was perpendicular to the blood vessel. In the current work the realistic geometry for the blood vessel and liver was reconstructed using the MRI images. We take the acoustic streaming effect into account with an aim to show that the incident finite-amplitude ultrasound wave can slightly affect the blood flow motion in large hepatic vessels.

The rest of this paper will be organized as follows. In Section 2 we present the three-field coupling model without considering the nonlinear acoustic effect. The physical domain will be split into the perfusion (tissue) and the convective cooling domains (blood vessel) so that the biologically relevant heat sinks can be modeled. In the blood domain, energy equation will be coupled with the nonlinear hemodynamic equations where the effect of acoustic streaming is included for the modeling of a finite-amplitude wave propagation. Our aim is to show that the incident finite-amplitude ultrasound wave can slightly affect the blood flow motion in large hepatic vessels. In Section 3 we will briefly describe the problem, in Section 4 the computational model, and then present in Section 5 the simulated results. Conclusions will be given in Section 6.

2. Three-field coupling model

Medical ultrasound, which is nothing but a mechanical wave having a frequency beyond the threshold value (16 kHz), can induce a slight matter oscillation. This type of longitudinal wave is generated by an in-unison movement of particles that contain many atoms. As these particles in a medium are displaced from their equilibrium locations, the electrostatic restoration force will be generated. The resulting internal force between the particles, together with the inertia of these particles, can cause the medium to oscillate. Medical ultrasound with a frequency of several MHz and a wavelength of order 1 mm, say for example, can penetrate our tissues well. In addition, it can compress and expand the tissues millions of times per second. Such a high-power ultrasound can penetrate deep into the tissues and, thus, makes it appealing for use in some non-invasive surgeries.

Intense ultrasound energy can be delivered to a small region of targeted tissue with a negligible effect on its surrounding area. Absorption of mechanical energy of this sort can, as a result, elevate tissue temperature to a certain high magnitude and can cause the thermal coagulation and ablation of cells to occur within a short time interval. For the sake of quantifying tissue response to an applied ultrasound, we need to take into account the biological structures in the region under current investigation.

2.1. Linear acoustic equation for ultrasound propagation

Due to the thermal-viscous loss in tissues, acoustic pressure can be expressed as $p = c_0^2 \rho + \frac{c_0^2}{\rho_0} \frac{\beta}{2A} \rho^2 + \dots$ [23]. This constitutive equation, which contains the ambient sound speed c_0 and the nonlinearity parameter $\frac{\beta}{2A}$ for fluids, stands for the relation between the sound pressure and density. Note that the medium of current interest is assumed to be homogeneous. As a result, the term accounting for medium inhomogeneity in density ρ , or $\frac{\nabla \rho}{\rho} \nabla p$, will be neglected in the current formulation of acoustic equation.

The resulting Westervelt wave equation [23] given below for ultrasound pressure p is employed for modeling the finite-amplitude nonlinear wave propagation in a soft tissue, which is modeled as a thermo-viscous fluid:

$$\nabla^2 p - \frac{1}{c_0^2} \frac{\partial^2 p}{\partial t^2} + \frac{\delta}{c_0^4} \frac{\partial^3 p}{\partial t^3} + \frac{\beta}{\rho_0 c_0^4} \frac{\partial^2 p}{\partial t^2} = 0 \quad (1)$$

The first two terms describe the linear lossless wave propagating at the small-signal sound speed. The third loss term is due to thermal conductivity and fluid viscosity. The last term accounts for acoustic nonlinearity which can affect the thermal and mechanical changes within the tissues [24]. In soft tissues, which are assumed to be thermoviscous, the acoustic diffusivity δ accounts for the thermal and viscous losses in a fluid and is modeled by

$$\delta = \frac{2c_0^3 \alpha}{\omega^2} \quad (2)$$

where α denotes the acoustic absorption coefficient. In Eq. (1), $\beta = 1 + \frac{B}{2A}$ and $\omega (\equiv 2\pi f)$ are the nonlinearity coefficient and the angular frequency, respectively.

As a first study towards HIFU application, we neglect the non-linear effect, which will be the focus of future study, for simplifying the analysis within the linear context. In our study each small element dS of the transducer surface vibrates continuously with the same velocity $u = u_0 \exp(i\omega t)$ normal to the surface. In this case the resulting linear wave equation $\nabla^2 p - \frac{1}{c_0^2} \frac{\partial^2 p}{\partial t^2} + \frac{\delta}{c_0^4} \frac{\partial^3 p}{\partial t^3} = 0$ can be transformed to the diffraction integral for the velocity potential as follows [25,26]

$$\psi_{\bar{p}} = \iint_S \frac{u}{2\pi r} \exp^{-(\alpha+ik)r} dS \quad (3)$$

In the above r is the distance from the source point on the transducer surface dS to a field point \bar{p} , and k is the wave number. The pressure amplitude at point \bar{p} can be calculated from the following expression

$$p_{\bar{p}} = ikc\rho_t \psi \quad (4)$$

where ρ_t is the density of tissue, and c is the speed of ultrasound in tissues.

The ultrasound power deposition per unit volume is assumed to be proportional to the local acoustic intensity I as follows

$$q = 2\alpha I \quad (5)$$

where the intensity I is defined as

$$I = \frac{p_{\bar{p}}^2}{2\rho_t c} \quad (6)$$

Note that Eqs. (3) and (4) take into account only the effects of diffraction and attenuation without considering the effect of nonlinearity. One can predict nonlinear acoustic pressure by means of Westervelt equation (1) or KZK wave equation. For the currently investigated transducer, with the aperture angle 30°, KZK equation is not recommended, since it can be applied only for directional sound beams with aperture angles <19°. Several studies [21,22,24,27–29] showed that for the focal intensities in the range of 100–1000 W/cm², the peak negative pressure in the range of 1–4 MPa and the nonlinearity parameter equal to few tenths, the complexities such as cavitation and highly nonlinear propagation can be neglected with acceptable errors. In the present study the acoustic energy emitted from the transducer is 50 W. The intensity generated at the focus is 300 W/cm². Therefore we do not consider here the effect of nonlinearity and cavitation.

Absorption and attenuation coefficients in tissue are normally increased with the frequency in power law form for most media [30]. This is the main reason of the increasing use of high-intensity ultrasound in tissue heating. The penetration depth of ultrasound is, on the other hand, limited by the frequency in accordance with Eq. (3). In this study we will consider three frequencies $f = 0.8, 1.0$ and 1.2 MHz.

2.2. Energy equation for tissue heating

Whereas hepatic arteries and portal veins irrigate the liver parenchyma, hepatic veins will drain blood out of the liver and can, thus, represent a heat sink. Tumor cells in perivascular region, as a result, may escape the externally imposed high heat, leading possibly to a local recurrence. This is also a major thermal equilibrium process that takes place in the pre- or post-capillary vessel. Therefore, the mathematical model appropriate for predicting the elevated temperature in tissues must take the heat conduc-

tion, tissue perfusion, convective blood cooling, and heat deposition due to an incident wave into account. In this paper we will develop a biologically more realistic thermal model by dividing the region of current interest into the region with tissue perfusion, which is due mainly to the capillary beds, and the capillary region containing blood vessels. In other words, the temperature field has been split into the domains for the perfused tissue and the flowing blood.

In a region free of large blood vessels, the diffusion-type Pennes bioheat equation [20] given below will be employed to model the transfer of heat in the perfused tissue region:

$$\rho_t c_t \frac{\partial T}{\partial t} = k_t \nabla^2 T - w_b c_b (T - T_\infty) + q \quad (7)$$

In the above energy equation proposed for modeling the time-varying temperature in the tissue domain, ρ , c , k denote the density, specific heat, and thermal conductivity, respectively, with the subscripts t and b referring to the tissue and blood domains. The notation T_∞ is denoted as the temperature at a location that is quite away from the heating focus. w_b ($\equiv 0.5 \text{ kg/m}^3 \text{ s}$) shown in Eq. (7) is known as the perfusion rate for the tissue cooling in capillary flows. It is noted that the above energy equation for T is coupled with the linear acoustic equation (4) for acoustic pressure through the power deposition term q defined in Eq. (5).

In the region containing large vessels, within which the flowing blood can convect heat, the biologically relevant heat source, which is q , and the heat sink, which is $-\rho_b c_b \underline{\mathbf{u}} \cdot \nabla T$, will be added to the conventional diffusion-type heat equation. The resulting modeling equation avoids a possible high recurrence stemming from the tumor cell survival next to large vessels

$$\rho_b c_b \frac{\partial T}{\partial t} = k_b \nabla^2 T - \rho_b c_b \underline{\mathbf{u}} \cdot \nabla T + q \quad (8)$$

where $\underline{\mathbf{u}}$ is the blood flow velocity. Owing to the presence of blood flow velocity vector $\underline{\mathbf{u}}$ in the above energy equation, we are led to know that a biologically sound model for the HIFU simulation comprises a coupled system of thermal–fluid–acoustics nonlinear differential equations in the sense that the heat sink is coupled with the hydrodynamic equations described later in Section 2.3 and the heat source is governed by the acoustic field equation described previously in Section 2.1.

Thermal dose developed by Sapareto and Dewey [31] will be applied to provide a quantitative relationship between temperature and time for the heating of tissue and the extent of cell killing. In focused ultrasound surgery (generally above 50 °C), the expression for the thermal dose (TD) can be written as:

$$TD = \int_{t_0}^{t_{final}} R^{(T-43)} dt \approx \sum_{t_0}^{t_{final}} R^{(T-43)} \Delta t \quad (9)$$

where $R = 2$ for $T \geq 43^\circ\text{C}$, $R = 4$ for $37^\circ\text{C} < T < 43^\circ\text{C}$. The value of TD required for total necrosis ranges from 25 to 240 min in biological tissues [31,32,29]. According to this relation, thermal dose resulting from heating the tissue to 43 °C for 240 min is equivalent to that achieved by heating it to 56 °C for one second.

2.3. Acoustic streaming hydrodynamic equations

Owing to the inclusion of heat sink, which is shown on the right hand side of (8), the velocity of the blood flow plus the velocity resulting from the acoustic streaming due to the applied high-intensity ultrasound must be determined. In this study we consider that the flow in large blood vessels is incompressible and laminar. The vector equation for modeling the blood flow motion, subject to the divergence free velocity $\nabla \cdot \underline{\mathbf{u}} = 0$, in the presence of acoustic stress is as follows [33,34].

$$\frac{\partial \underline{\mathbf{u}}}{\partial t} + (\underline{\mathbf{u}} \cdot \nabla) \underline{\mathbf{u}} = \frac{\mu}{\rho} \nabla^2 \underline{\mathbf{u}} - \frac{1}{\rho} \nabla \mathbf{P} + \frac{1}{\rho} \underline{\mathbf{F}} \quad (10)$$

where \mathbf{P} is the static pressure, μ ($= 0.0034 \text{ kg/m s}$) the shear viscosity of blood flow, and ρ the blood density. In Eq. (10), the force vector $\underline{\mathbf{F}}$ acting on the vessel blood fluid due to ultrasound is assumed to propagate along the acoustic axis $\underline{\mathbf{n}}$. The resulting nonzero component in $\underline{\mathbf{F}}$ takes the following form [35]

$$\underline{\mathbf{F}} \cdot \underline{\mathbf{n}} = \frac{2\alpha}{c_0} I \quad (11)$$

The acoustic intensity I shown above has been defined in Eq. (6). Amongst the second-order physical effects, only the acoustic streaming will be taken into account.

3. Description of the problem

In Figs. 1, 2 the 3D-reconstructed liver model contains a patient's hepatic artery and an artificial spherical solid tumor with the radius of 0.01 m. The HIFU transducer used in this study is a single element, spherically focused with a diameter of 10 cm and a radius of curvature of 10 cm [36]. A piezoelectric transducer presumably emits a beam of spherically-shaped ultrasound wave towards the targeted tissue under current investigation. The parameters used in the simulation are listed in Table 1 [35,37,32,10].

Here we consider the case with linear dependence of attenuation coefficient on frequency [37,38]. In this study, the ultrasound of 1 MHz insonation is incident from a location that is exterior of the liver tumor with a diameter of 10 cm. The acoustic energy emitted from the transducer is 50 W.

Initially, we consider that the temperature is equal to 37 °C and the blood flows at 0.06 m/s on the inlet vessel plane. Typically, pulse duration is in the range of 1–10 s [36,22]. The solid tumor was entirely exposed to a 8-s ultrasound. To see how the temperature will be changed under different ultrasound frequencies, we chose three frequencies, which are 0.8 MHz, 1.0 MHz and 1.2 MHz.

4. Computational model

The present numerical experiments are carried out in a patient-specific liver model. Contour shape of the liver is a priori known as a closed regular surface that is considered as an elastic surface in

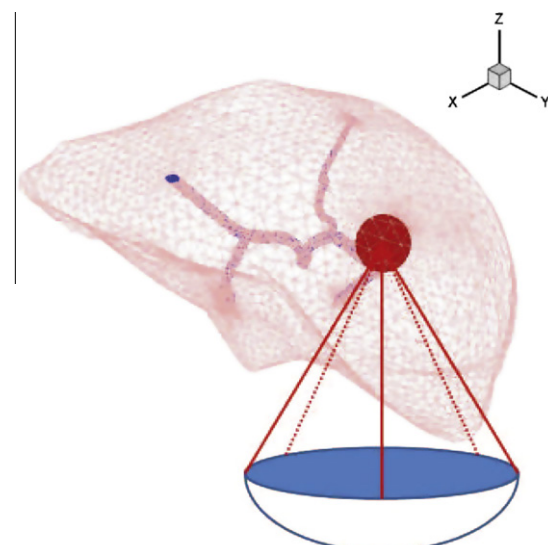


Fig. 1. Schematic of the physical model, which contains the liver, solid tumor, and artery.

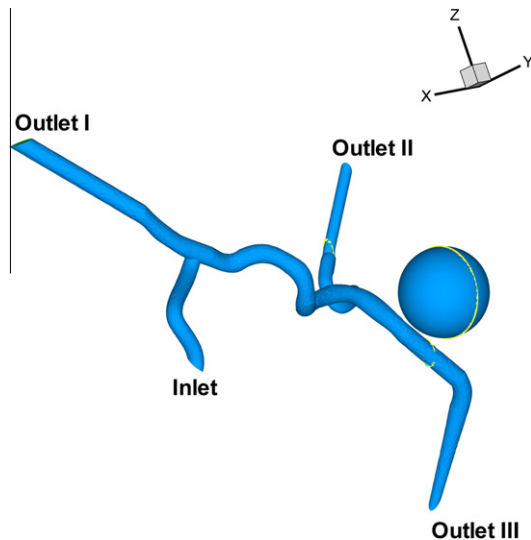


Fig. 2. Schematic of the inlet and outlets of the investigated hepatic arterial vessel.

Table 1
Acoustic and thermal properties for the liver tissue, tumor and blood.

Tissue	$c \left(\frac{\text{m}^3}{\text{s}} \right)$	$\rho \left(\frac{\text{kg}}{\text{m}^3} \right)$	$c \left(\frac{1}{\text{kg K}} \right)$	$k \left(\frac{\text{W}}{\text{m K}} \right)$	$\alpha \left(\frac{\text{Np}}{\text{m}} \right)$
Tumor [10]	1550	1000	3800	0.552	9 *f
Liver [32,37]	1550	1055	3600	0.512	9 *f
Blood [37,35]	1540	1060	3770	0.53	1.5 *f

equilibrium under a set of forces. Liver surface mesh is directly generated by starting from an average template mesh that is deformed onto the image set. Surface mesh merging onto the surface of the liver was carefully controlled on zoomed medical images. Volumetric mesh is generated using the INRIA software TetMesh [39]. The arterial network also derives from a 3D reconstruction of an arterial segment.

The three-dimensional problem involving liver, tumor and blood vessel will be analyzed using well-developed commercially available CFDRC (CFD Research, Huntsville, AL, USA) software for gaining the physical insight. Referring to Fig. 1, the non-uniform refined grids were generated near the boundaries of the tumor, blood vessel. The number of grids used in the present study was 81,608 in tumor, 122,236 in blood vessel, and 381,301 in liver.

The upwind numerical scheme for the velocity derivatives and 2nd order scheme for the temperature for spatial derivatives were used. The time step was 0.05 s. The number of steps employed in the current studies was 500. The AMG (Algebraic Multi Grid) algorithm was also used for enhancing the pressure–velocity coupling and for improving the pressure correction. Conjugate gradient squared + preconditioning (CGS + Pre) solver was used for the temperature field. In all the investigations, the iterative calculations of the field variables were terminated when all the residual norms become smaller than 10^{-10} .

Mesh independence was assessed by comparing the temperature distribution in the final working mesh with the temperature obtained in a refined mesh. After increasing the number of cells by 30% we found that the temperature distribution varies less than by 1%. Temperature in the center of tumor was independently calculated by FreeFem++ and compared with the CFDRC solution.

Detailed descriptions about the CFD code and the solution procedures can be found in the CFDRC manual (2003). In the final stage, the predicted results were viewed and analyzed by the

three-dimensional animated plotting tools such as the CFD-VIEW and TecPlot.

5. Numerical results

The proposed three-field coupling mathematical model in Section 2 will be used to get the temperature distribution in the tumor. First we will study temperature distribution in the tumor, when the focal point is in the center of tumor for different frequencies.

In Fig. 3 we present the power deposition per unit volume (ultrasound power density) as the function of distance measured from the transducer at the focal axis for three different frequencies. We can see that at higher frequency we have larger power deposition per unit volume in the focal point, but the region with large power deposition is narrower. In Figs. 4–7 we can see the computed temperature contours in the tumor and liver at the cutting plane $y = 0$ for $t = 3, 5, 8$ s and at the cutting plane $z = 0.1$ for $t = 8$ s. While the highest temperature is present inside the tumor, although the liver has a small temperature arise, it will not cause the liver tissue to necrosis. In these figures we do not show the simulated temperature contours with the magnitudes higher than 56 °C, because as we mentioned before it is the threshold value for the tissue necrosis.

In Fig. 4 we can see that for $t = 3$ s the region with the temperature higher than 56 °C is larger for the transducer with frequency $f = 1.0$ MHz, than for the frequency $f = 1.2$ MHz. The smallest region is for the frequency $f = 0.8$ MHz. At a time $t \geq 5$ s, we can see that the higher the ultrasound frequency, the smaller the focused region of higher temperature. In Fig. 8 we can see the predicted thermal doses at different frequencies. For the discussion of the dependence of temperature on time at different frequencies we have chosen several points, schematic in Fig. 9, inside the tumor along the focal axis z and several points close to the focal point $z = 0.1$ along the axis y . The results are presented in Figs. 10 and 11.

At the focal point ($z = 0.1$), in accordance with the power deposition distribution per unit volume in Fig. 3, in the first three seconds of heating, the predicted temperature for 1.2 MHz transducer is slightly higher than the temperatures for the 0.8 and 1.0 MHz transducers. At a time $t > 3$ s the temperature for 1.0 MHz transducer becomes higher than for 1.2 MHz. It is caused by a heat conduction. The region with larger power deposition per

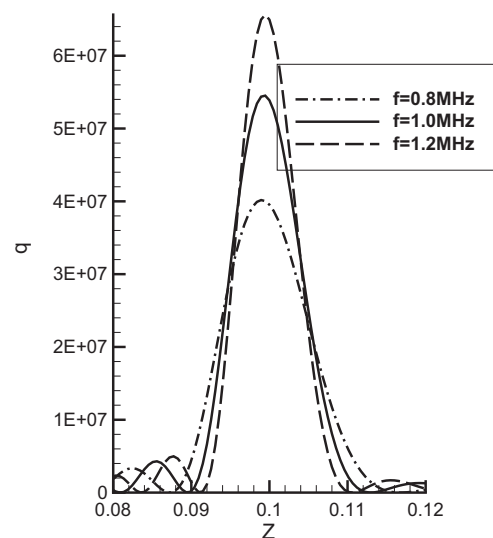


Fig. 3. The predicted power depositions per unit volume plotted against the axial distance for the cases considered at three different frequencies.

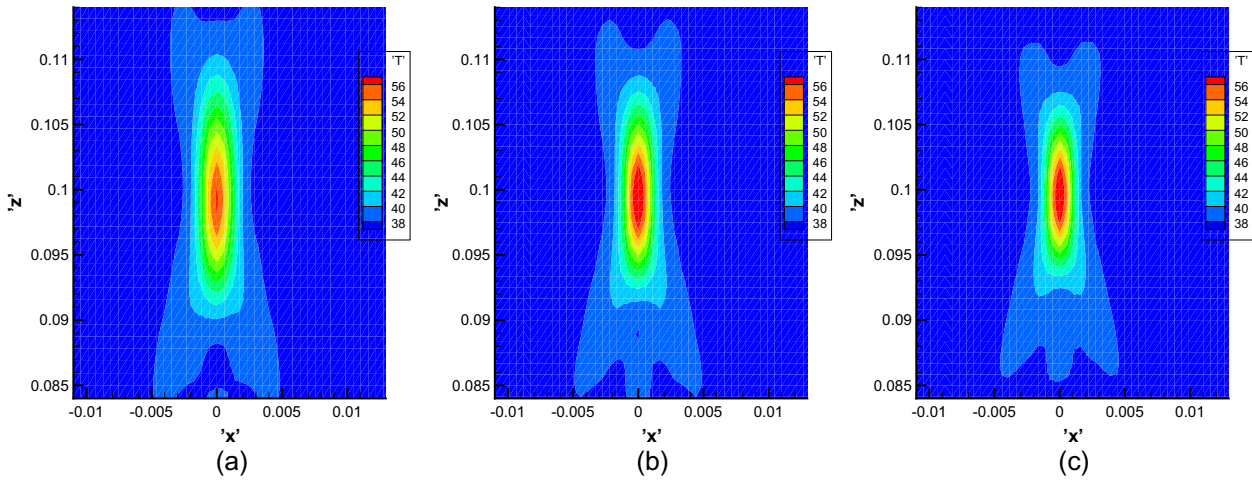


Fig. 4. The predicted temperature contours in the tumor (3 s). (a) $f = 0.8$ MHz; (b) $f = 1.0$ MHz and (c) $f = 1.2$ MHz.

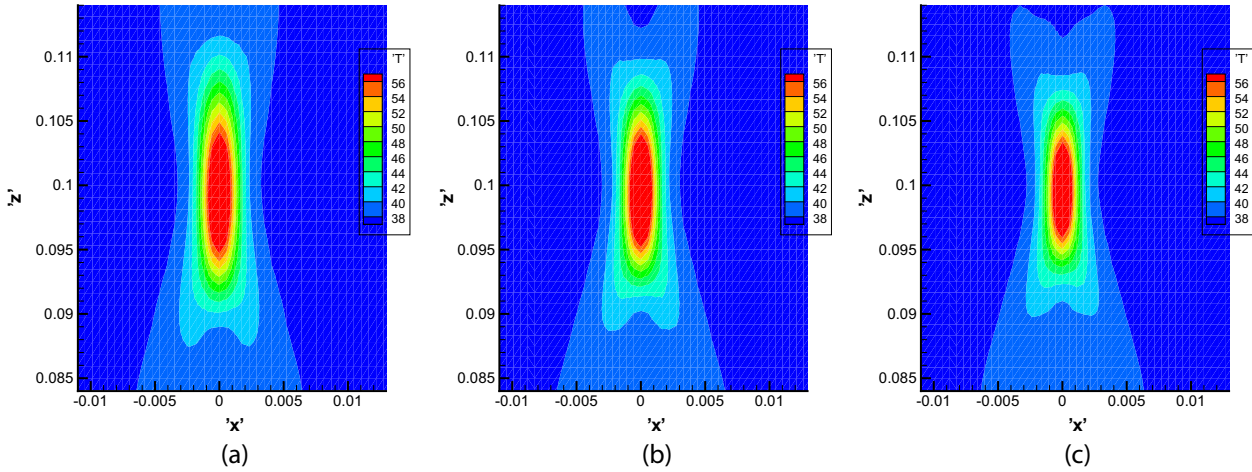


Fig. 5. The predicted temperature contours in the tumor (5 s). (a) $f = 0.8$ MHz; (b) $f = 1.0$ MHz and (c) $f = 1.2$ MHz.

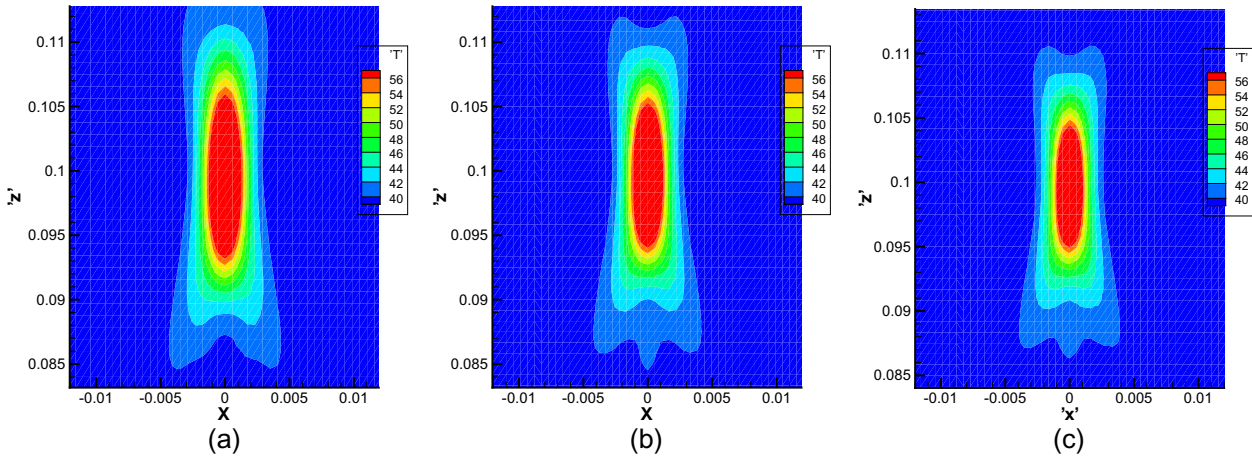


Fig. 6. The predicted temperature contours in the tumor (8 s). (a) $f = 0.8$ MHz; (b) $f = 1.0$ MHz and (c) $f = 1.2$ MHz.

unit volume is narrower for higher frequency. Near the surrounding area, the temperature is lower, but the temperature gradient is high.

We can see the similar behavior at the distance 2 cm from the focal point. For the first two seconds the temperature is almost

the same for $f = 1.0$ and 1.2 MHz. However, $T_{1.0} > T_{0.8} > T_{1.2}$ at $t = 8$ s. At a larger distance from the focal point, the temperature for 0.8 MHz transducer becomes higher.

Along the y direction the temperature changes faster than that along the focal axis. At the distances 1 and 2 mm from the focal

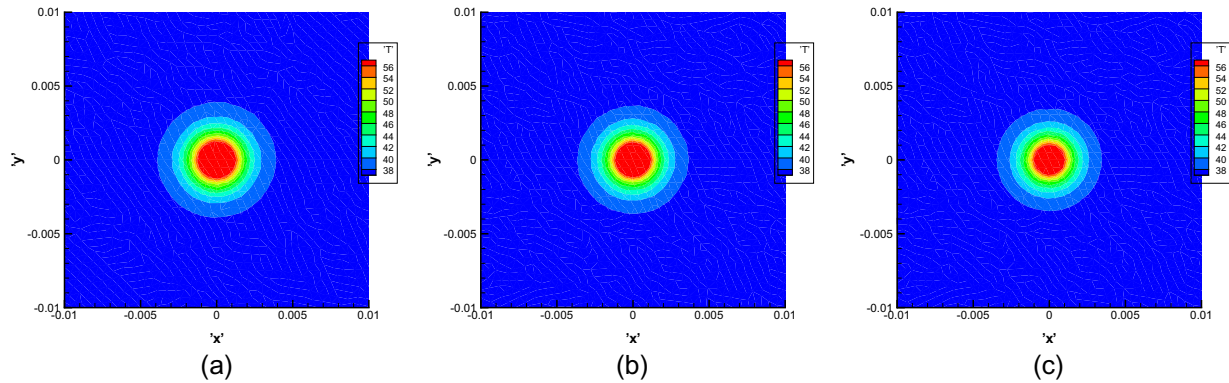


Fig. 7. The predicted temperature contours in the tumor at the cutting plane $z = 0.1$ (8 s). (a) $f = 0.8 \text{ MHz}$; (b) $f = 1.0 \text{ MHz}$ and (c) $f = 1.2 \text{ MHz}$.

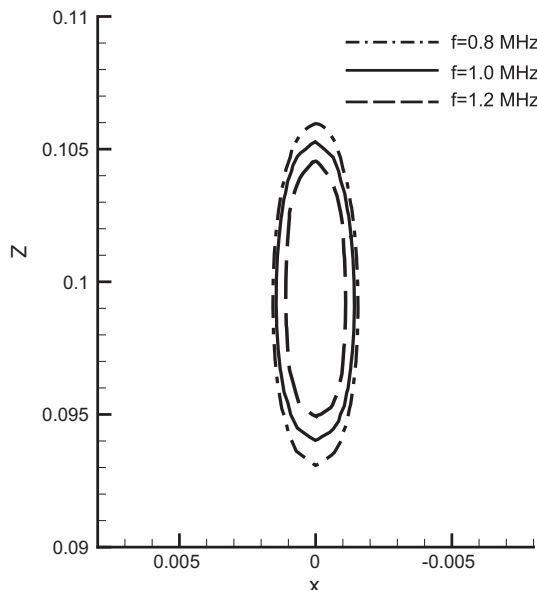


Fig. 8. The predicted lesion areas in the xz plane (or plane $y = 0$). Lesion boundaries are extracted from the thermal dose contours based on the threshold value of 240 min.

point, presented in Fig. 11, the temperature predicted from the 0.8 MHz transducer is higher than those for 1.0 MHz and 1.2 MHz transducers. At the distance $y = 2 \text{ mm}$ we can see that the highest temperature is at time $t \approx 10 \text{ s}$, while the sonication time is 8 s . It is caused by heat conduction from the region with the higher temperature.

For $f = 0.8 \text{ MHz}$ we get more uniform temperature distribution in the tumor and the tumor lesion volume becomes larger. This means that this ultrasound frequency is more suitable for the ablation of tumor. In Table 2 we can see that due to the dependence of attenuation on frequency, the higher the ultrasound frequency, the less amount of heat is absorbed in the liver tumor.

5.1. The effect of blood flow

When the focal point is at the center of tumor, cooling effect due to the blood flow motion does not play an important role in the temperature distribution inside the tumor, because of the relatively large distance (about 1.5 cm) between the focal point and the vessel. In this case we can ignore the effect of blood flow. Let's consider next the case when the focal point is closer to the boundary of the tumor and near the blood vessel.

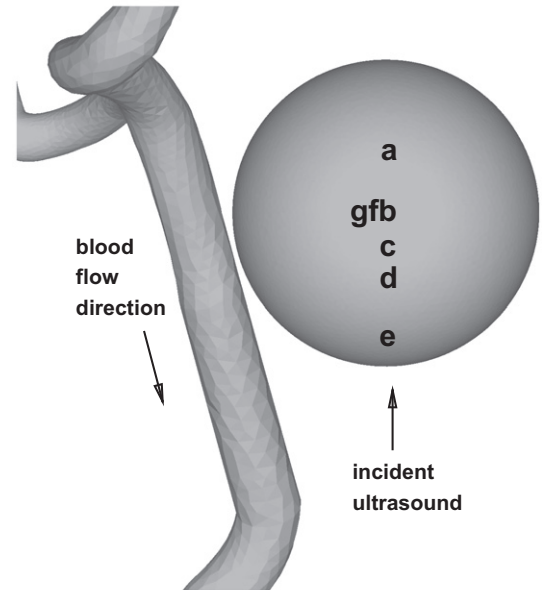


Fig. 9. Schematic of the chosen locations at which temperature will be plotted against time.

In Figs. 12 and 13 we can see the spatial temperature distributions for different frequencies at $t = 8 \text{ s}$. We can conclude that blood vessel should be taken into account in this case. However there is only a small change in the lesion size (about 3%). When the blood vessel becomes closer to the focal point the effect becomes more pronounced. In Table 2 we present the calculated energy in tumor for two cases, when the focal point is in the center of tumor and when the focal point is at the boundary in the tumor. Since the dependence of attenuation coefficients of frequency is linear, the higher the frequency of transducer the less energy is delivered to the tumor.

5.2. The effect of acoustic streaming

Acoustic streaming is considered as a second order physical effect in the HIFU therapy and is usually neglected. To investigate the importance of acoustic streaming effect during the thermal therapy, we have calculated hydrodynamic equation (10) with and without acoustic source given in (11). In Table 3 we present the predicted mass fluxes at the inlet and three outlets, schematic in Fig. 2, with and without acoustic streaming. We can see that mass

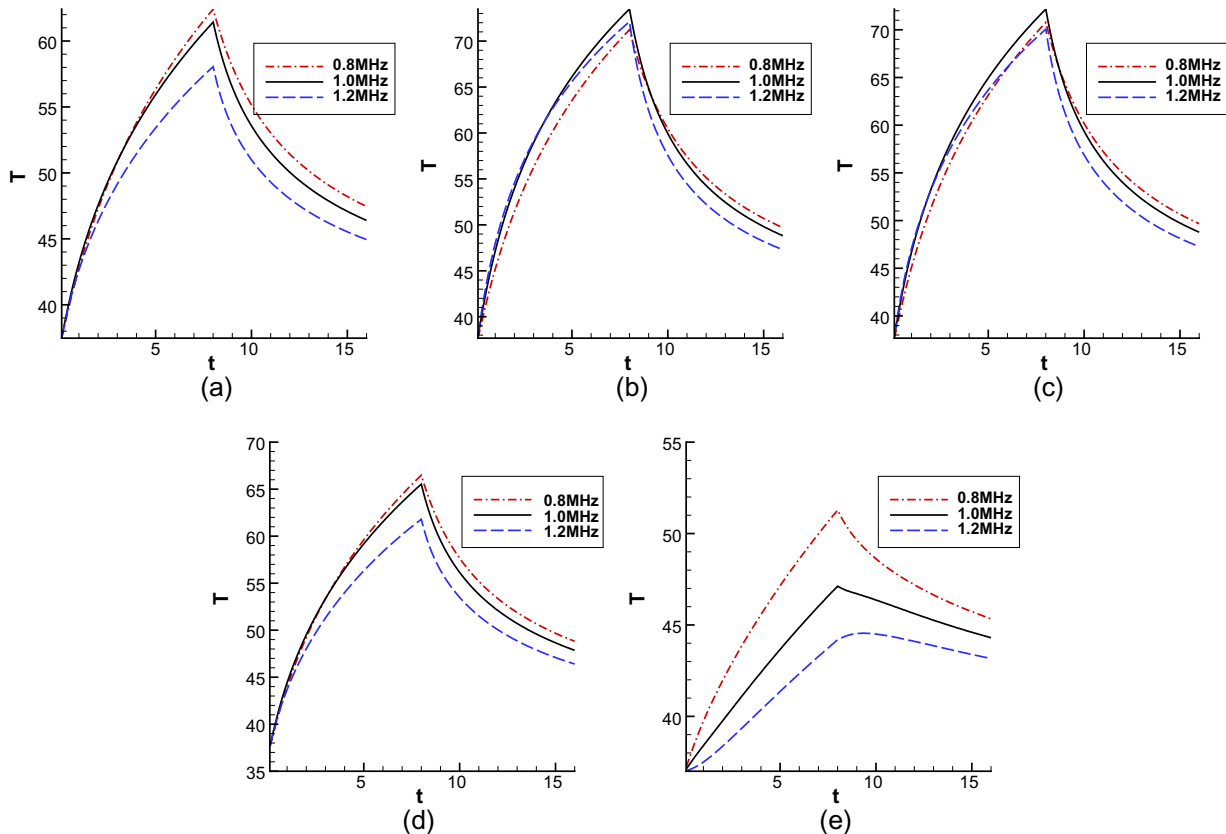


Fig. 10. The predicted temperature distributions at different focal axis points for the cases investigated at three different frequencies. (a) $z = 0.104$ m; (b) $z = 0.1$ m; (c) $z = 0.098$ m; (d) $z = 0.96$ m and (e) $z = 0.92$ m.

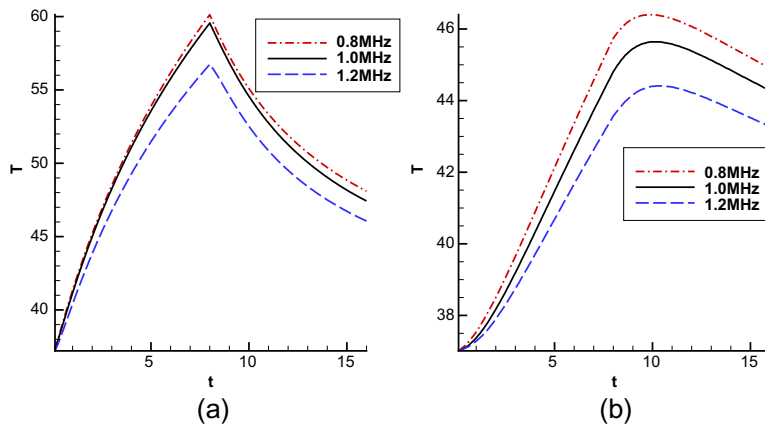


Fig. 11. The predicted temperature distributions at different points along y axis near the focal point for the cases investigated at three different frequencies. (a) $y = 0.001$ m and (b) $y = 0.002$ m.

Table 2

Energy in the tumor. (A) Focal point is in the center of tumor and (B) focal point is at the boundary of the tumor, close to the blood vessel.

Frequency (MHz)	Energy in the tumor (A) (W)	Energy in the tumor (B) (W)
0.8	3.33	2.13
1.0	2.93	1.99
1.2	2.53	1.77

fluxes at outlets can be redistributed and the acoustic streaming effect cannot be ignored because it can cause a considerable redistribution of the mass flux, up to 16% in our case. This effect can be

also used to control drug delivery. Calculations of the temperature with and without acoustic streaming effect show that acoustic streaming can affect the temperature distribution only by a negligible amount. The distance between the focal point and blood vessel is about 1 cm. For the case with a closer distances between the blood vessel and the tumor the importance of acoustic streaming will increase.

6. Concluding remarks

We have proposed a three dimensional physical model for the HIFU study conducted in a patient specific liver geometry. The

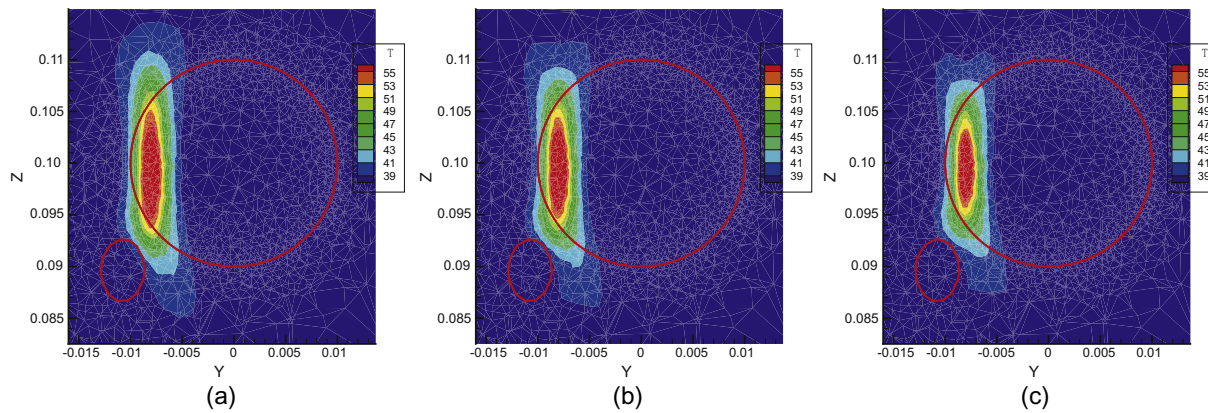


Fig. 12. The predicted temperature contours in the tumor at the cutting plane $x = 0$ for the cases investigated at different frequencies (5 s). (a) $f = 0.8$ MHz; (b) $f = 1.0$ MHz and (c) $f = 1.2$ MHz.

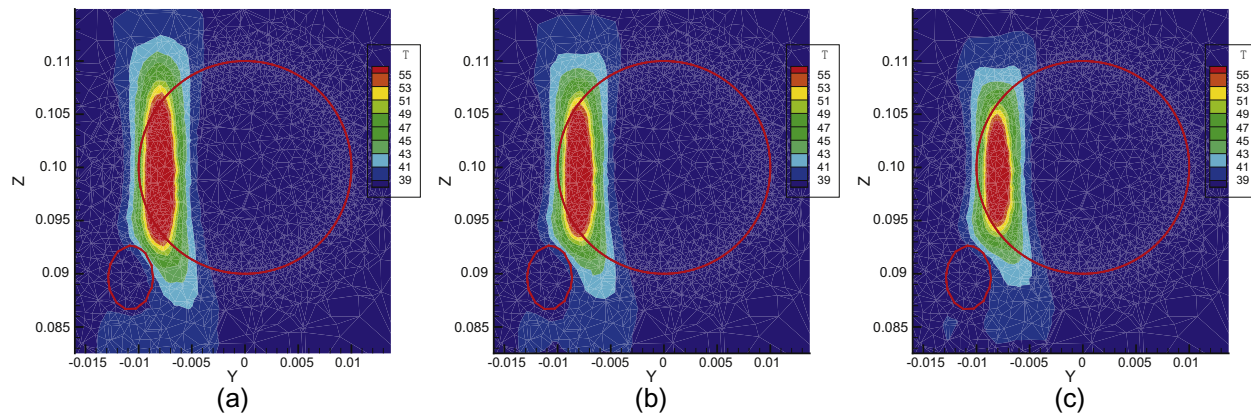


Fig. 13. The predicted temperature contours in the tumor at the cutting plane $x = 0$ for the cases investigated at different frequencies (8 s). (a) $f = 0.8$ MHz; (b) $f = 1.0$ MHz and (c) $f = 1.2$ MHz.

Table 3
Acoustic streaming effect on the mass flux. Mass flux (kg/s).

Tissue	Outlet 1	Outlet 2	Outlet 3	Inlet
Without AS	5.31×10^{-4}	6.29×10^{-5}	1.64×10^{-4}	7.58×10^{-4}
With AS	5.50×10^{-4}	7.11×10^{-5}	1.37×10^{-4}	7.58×10^{-4}
Difference	+3.6%	+13.0%	-16.5%	

proposed model takes into account the convective cooling in large blood vessel and the perfusion due to capillary flows. Acoustic streaming was also included in the simulation model. Convective cooling in large blood vessel and acoustic streaming were shown to change the temperature near blood vessel. Acoustic streaming effect can affect the blood flow distribution in hepatic arterial branches and lead to a mass flux redistribution. This effect can be used to control drug delivery. It is necessary to take into account both the convective cooling and acoustic streaming effects in large blood vessel, when the tumor is close to large blood vessel.

HIFU frequency has been shown to affect the heat deposition on the tumor. The higher the ultrasound frequency, the less amount of the heat is absorbed in the liver tumor. The higher the ultrasound frequency, the smaller the focused region of the higher temperature. We showed that the most proper frequency for the three investigated transducers is 0.8 MHz. It is necessary to take into account the effect of frequency in the design of transducers for HIFU applications.

These results can be further used to construct a surgical planning platform for the non-invasive HIFU (High-Intensity Focal

Ultrasound) tumor ablating (or cauterizing) therapy in real liver geometry on the basis of the MRI image.

Acknowledgements

The authors would like to acknowledge the financial support from the National Science Councils under the projects NSC 99-2628-M-002-005 and NSC 97-2221-E-002-250-MY3. The authors will also thank Prof. W.L. Lin for his valuable comments made in the course of conducting this study.

References

- [1] M. Thiriet, *Biology and Mechanics of Blood Flows. Part I: Biology*, Springer, New York, 2008.
- [2] The Liver Cancer Study Group Of Japan. Primary liver cancer in Japan, Sixth report, *Cancer* 60 (1987) 1400–1411.
- [3] J.S. Huang, D.A. Gervais, P.R. Mueller, Radiofrequency ablation: review of mechanism, indications, technique, and results, *Chinese J. Radiol.* 26 (2001) 119–134.
- [4] S.A. Curley, F. Izzo, P. Delrio, L.M. Ellis, J. Granchi, P. Vallone, F. Fiore, S. Pignata, B. Banielle, F. Cremona, Radiofrequency ablation of unresectable primary and metastatic hepatic malignancies: results in 123 patients, *Ann. Surgery* 230 (1999) 1–8.
- [5] G. Steele, T.S. Ravikumar, Resection of hepatic metastases from colorectal cancer, *Ann. Surgery* 210 (1989) 127–138.
- [6] S. Tungjitkusolmun, S.T. Staelin, D. Haemmerich, J.Z. Tasi, H. Cao, J.G. Webster, F.T. Lee, D.M. Mahvi, V.R. Vorperian, Three-dimensional finite-element analysis for radio-frequency hepatic tumor ablation, *IEEE Trans. Biomed. Eng.* 49 (1) (2002) 3–9.
- [7] S.M. Lin, D.Y. Lin, Percutaneous local ablation therapy in small hepatocellular carcinoma, *Chang Gung Med. J.* 26 (5) (2003) 308–313.

- [8] J.P. McGaham, P.D. Browning, J.M. Brock, H. Tesluk, Hepatic ablation using radiofrequency electrocautery, *Investigat. Radiol.* 25 (1990) 267–270.
- [9] S.A. Curley, F. Izzo, L.M. Ellis, J.N. Vauthey, P. Vallone, Radiofrequency ablation of hepatocellular cancer in 110 patients with cirrhosis, *Ann. Surgery* 232 (2000) 381–391.
- [10] T.W.H. Sheu, C.W. Chou, S.F. Tsai, P.C. Liang, Three-dimensional analysis for radiofrequency ablation of liver tumor with blood perfusion effect, *Comput. Methods Biomed. Eng.* 8 (4) (2005) 229–240.
- [11] C.C. Coussios, C.H. Farny, G. Ter Haar, R.A. Roy, Role of acoustic cavitation in the delivery and monitoring of cancer treatment by high-intensity focused ultrasound (HIFU), *Int. J. Hyperthermia* 23 (2) (2007) 105–120.
- [12] T.A. Leslie, J.E. Kennedy, High intensity focused ultrasound in the treatment of abdominal and gynaecological diseases, *Int. J. Hyperthermia* 23 (2007) 173–182.
- [13] F. Wu, Z.B. Wang, W.Z. Chen, W. Wang, Y. Gui, M. Zhang, G. Zheng, Y. Zhou, G. Xu, M. Li, C. Zhang, H. Ye, R. Feng, Extracorporeal high intensity focused ultrasound ablation in the treatment of 1038 patients with solid carcinomas in China: An overview, *Ultrason. Sonochem.* 11 (2004) 149–154.
- [14] F. Wu, Z.B. Wang, W.Z. Chen, H. Zhu, J. Bai, J.Z. Zou, K.Q. Li, C.B. Jin, F.L. Xie, H.B. Su, Extracorporeal high intensity focused ultrasound ablation in the treatment of patients with large hepatocellular carcinoma, *Ann. Surg. Oncol.* 11 (2004) 1061–1069.
- [15] J.E. Kennedy, F. Wu, G.R. ter Haar, F.V. Gleeson, R.R. Phillips, M.R. Middleton, D. Cranston, High-intensity focused ultrasound for the treatment of liver tumours, *Ultrasonics* 42 (2004) 931–935.
- [16] R.O. Illing, J.E. Kennedy, F. Wu, G.R. ter Haar, A.S. Protheroe, P.J. Friend, F.V. Gleeson, D.W. Cranston, R.R. Phillips, M.R. Middleton, The safety and feasibility of extracorporeal high-intensity focused ultrasound (HIFU) for the treatment of liver and kidney tumours in a Western population, *Br. J. Cancer* 93 (2005) 890–895.
- [17] S. Wang, Extracorporeal high-intensity focused ultrasound treatment for a child with recurrence of hepatocellular carcinoma, *Eur. J. Radiol. Extra* (2010), in press, doi:10.1016/j.ejrex.2010.06.003.
- [18] F. Wu, Z.B. Wang, P. Lu, et al., Activated anti-tumor immunity in cancer patients after high intensity focused ultrasound ablation, *Ultrasound Med. Biol.* 30 (9) (2004) 1217–1222.
- [19] L. Zhang, H. Zhu, C. Jin, K. Zhou, K. Li, H. Su, W. Chen, J. Bai, Z. Wang, High-intensity focused ultrasound (HIFU): effective and safe therapy for hepatocellular carcinoma adjacent to major hepatic veins, *Eur. Radiol.* 19 (2009) 437–445.
- [20] H.H. Pennes, Analysys of tissue and arterial blood temperature in the resting human forearm, *J. Appl. Physiol.* 1 (2) (1948) 93–122.
- [21] F.P. Curra, P.D. Mourad, V.A. Khokhlova, R.O. Cleveland, L.A. Crum, Numerical simulations of heating patterns and tissue temperature response due to high-intensity focused ultrasound, *IEEE Trans. Ultrason. Ferroelectr. Freq. Control* 47 (2000) 1077–1089.
- [22] P. Hariharan, M.R. Myers, R.K. Banerjee, HIFU procedures at moderate intensities – effect of large blood vessels, *Phys. Med. Biol.* 52 (12) (2007) 3493–3513.
- [23] M.F. Hamilton, D.T. Blackstock, *Nonlinear Acoustics*, Academic Press, Boston, 1998.
- [24] M. Bailey, V. Khokhlova, O. Sapozhnikov, S. Kargl, L. Crum, Physical mechanism of the therapeutic effect of ultrasound (A review), *Acoust. Phys.* 49 (4) (2003) 369–388.
- [25] A.D. Pierce, *Acoustics. An Introduction to its Physical Principles and Applications*, McGraw-Hill, New York, 1981.
- [26] H.T. O'Neil, Theory of focusing radiators, *J. Acoust. Soc. Am.* 21 (5) (1949) 516–526.
- [27] I. Hallaj, R. Cleveland, FDTD simulation of finite-amplitude pressure and temperature fields for biomedical ultrasound, *J. Acoust. Soc. Am.* 105 (5) (1999) L7–L12.
- [28] E.A. Filonenko, V.A. Khokhlova, Effect of acoustic nonlinearity on heating of biological tissue by high-intensity focused ultrasound, *Acoust. Phys.* 47 (4) (2001) 468–475.
- [29] P.M. Meaney, M.D. Cahill, G.R. ter Haar, The intensity dependence of lesion position shift during focused ultrasound surgery, *Ultrasound Med. Biol.* 26 (3) (2000) 441–450.
- [30] C.R. Hill, J.C. Bamber, G.R. Haar, *Physical Principles of Medical Ultrasonics*, John Wiley and Sons, 2004.
- [31] S.A. Sapareto, W.C. Dewey, Thermal dose determination in cancer therapy, *Int. J. Radiat. Oncol. Biol. Phys.* 10 (6) (1984) 787–800.
- [32] H.L. Liu, H. Chang, W.S. Chen, T.C. Shih, J.K. Hsiao, W.L. Lin, Feasibility of transrib focused ultrasound thermal ablation for liver tumors using a spherically curved 2D array: A numerical study, *Med. Phys.* 34 (9) (2007) 3436–3448.
- [33] T. Kamakura, M. Matsuda, Y. Kumamoto, M.A. Breazeale, Acoustic streaming induced in focused Gaussian beams, *J. Acoust. Soc. Am.* 97 (1995) 2740–2746.
- [34] K. Matsuda, T. Kamakura, Y. Kumamoto, Build up of acoustic streaming in focused beams, *Ultrasonics* 34 (1996) 763–765.
- [35] J. Huang, R.G. Holt, R.O. Cleveland, R.A. Roy, Experimental validation of a tractable medical model for focused ultrasound heating in flow-through tissue phantoms, *J. Acoust. Soc. Am.* 116 (4) (2004) 2451–2458.
- [36] T.C. Shih, H.L. Liu, K.C. Ju, C.S. Huang, P.Y. Chen, H.W. Huang, Y.J. Ho, The feasibility of heating on tumor periphery by using high intensity focused ultrasound thermal surgery, *Int. Comm. Heat Mass Transfer* 35 (2008) 439–445.
- [37] F.A. Duck, *Physical Property of Tissues - A comprehensive reference book*, Academic, London, 1990.
- [38] H.L. Liu, C.L. Hsu, S.M. Huang, Y.W. Hsi, Focal beam distortion and treatment planning for transrib focused ultrasound thermal therapy: A feasibility study using a two-dimensional ultrasound phased array, *Med. Phys.* 37 (2) (2010) 848–860.
- [39] P.L. George, Tetmesh-GHS3D, Tetrahedral Mesh Generator. INRIA Users Manual, INRIA (Institut National de Recherche en Informatique et Automatique), Rocquencourt, France, 2004.